Commutation Failure Mitigation Method Based on Imaginary Commutation Process

Renlong Zhu, Xiaoping Zhou, Haitao Xia, Lerong Hong, Hanhang Yin, Lingfeng Deng,
and Yifeng Liu

Abstract—**The commutation failure (CF) mitigation effectiveness is normally restricted by the delay of extinction angle (EA) measurement or the errors of existing prediction methods for EA or firing angle (FA). For this purpose, this paper proposes a CF mitigation method based on the imaginary commutation process. For each sample point, an imaginary commutation process is constructed to simulate the actual commutation process. Then, the imaginary EA is calculated by comparing the imaginary supply voltage-time area and the imaginary demand voltage-time area, which can update the imaginary EA earlier than the measured EA. In addition, the proposed method considers the impacts of commutation voltage variation, DC current variation, and phase angle shift of commutation voltage on the commutation process, which can ensure a more accurate EA calculation. Moreover, the DC current prediction is proposed to improve the CF mitigation performance under the single-phase AC faults. Finally, the simulation results based on CIGRE model prove that the proposed method has a good performance in CF mitigation.**

Index Terms—**Commutation failure (CF), commutation failure mitigation, extinction angle, line commutated converter based high-voltage direct current (LCC-HVDC).**

I. INTRODUCTION

LINE commutated convert based high-voltage direct current (LCC-HVDC) is widely used in power grid due to the growing demand of long-distance bulk power transmission [1], [2]. LCC-HVDC is superior to voltage-source converter based high-voltage direct current (VSC-HVDC) in transmission capacity, power losses, and investment benefits for long-distance bulk power transmission [3]. Yet, the commutation failure (CF) is an adverse and frequent phenomenon at the inverter side of LCC-HVDC system under the fault conditions [4]. The subsequent CF may easily occur if the first CF is not handled timely and correctly, which will result in the power outage and greatly affect the safe and stable operation of power grids [5], [6].

There are a lot of studies on the CF mechanism. It can be concluded that CFs are mainly caused by AC voltage disturbance such as AC voltage reduction, phase angle shift, and AC voltage distortion [7]-[9]. Since the AC voltage disturbance cannot be completely avoided, it is necessary to develop appropriate control methods to mitigate CF. The conventional voltage-dependent current order limiter (VDCOL) and the improved VDCOL [10]-[12] have been proposed in LCC-HVDC to reduce the risk of CF and improve the fault recovery performance by limiting the DC current order after the fault occurs. However, the CF mitigation capability of the system is restricted by the transmission delay of the DC current order from the inverter to the rectifier and the control delay of DC current. In addition, the advancing firing angle (FA) control is proposed to improve the control performance of the constant extinction angle (CEA) controller. The CEA controller can be classified into two categories: one is the measured-type controller such as CIGRE control [13] and SIEMENS control [14], [15], and the other is the predicted-type controller such as ABB control [15], [16] and the proposed methods in [17]-[20].

The measured-type CEA controller calculates the extinction angle (EA) by measuring the ending time of commutation process and the zero-crossing time of commutation voltage, which can obtain an accurate EA. However, the EA is only updated when the commutation voltage crosses zero, leading to a conspicuous control lag. Thus, the CF mitigation capability of the measured-type CEA controller is poor.

The predicted-type CEA controller calculates the EA using electric quantities such as DC current, commutation voltage, and commutation inductance. The predicted EA can be updated when the electric quantities have a change. Therefore, the predicted-type CEA controller reacts more quickly than the measured-type CEA controller. However, in ABB control, the error between the predicted EA and the actual EA is conspicuous under the fault conditions because the remarkable variation of the voltage-time area is neglected after the fault [15]. Moreover, the CF prevention (CFPREV) control [17] is added in ABB control to mitigate CF by immediately advancing the FA when AC faults are detected, but the CF mitigation performance of CFPREV needs to be improved by pa-

---

Manuscript received: September 5, 2021; revised: November 16, 2021; accepted: March 15, 2022. Date of CrossCheck: March 15, 2022. Date of online publication: June 8, 2022.

This work was supported by the Science and Technology Innovation Major Project of Hunan Province (No. 2020GK1010), the Innovation Young Talents Program of Changsha Science and Technology Bureau (No. kq2107005), and the Postgraduate Scientific Research Innovation Project of Hunan Province (No. QL20210101).

R. Zhu, X. Zhou (corresponding author), H. Xia, L. Hong, H. Yin, L. Deng, and Y. Liu are with the College of Electrical and Information Engineering, Hunan University, Changsha 410082, China (e-mail: 635107372@qq.com; zxp2011@hnu.edu.cn; xht0903@163.com; hlr0908@163.com; 296262037@qq.com; 2982766254@qq.com; 57340757@qq.com).

DOI: 10.35833/MPCE.2021.000611

rameter tuning. Reference [18] proposes an FA prediction method considering the DC current variation. However, the overlap angle (OA) is overestimated, which leads to an unnecessary increase in the reactive power consumption of inverter. Reference [19] proposes a calculation method of pseudo-EA, which can be used as a direct control variable to realize the real-time CEA control and CF mitigation. However, in [19], the FA shift is neglected, and the effectiveness in CF mitigation under single-phase AC faults is limited.

In this paper, a CF mitigation method is proposed based on the imaginary commutation process. Considering the impact of commutation voltage variation, DC current variation, and the phase angle shift of commutation voltage, the imaginary EA is calculated by the imaginary commutation process. Moreover, the DC current prediction is added to the proposed method to predict the imaginary EA in advance. The imaginary EA is selected as the input of CEA controller, together with the measured EA. Under the fault conditions, the proposed method can calculate the EA timely and can decrease the FA through the CEA controller to ensure a sufficient commutation margin.

The remainder of this paper is organized as follows. In Section II, the proposed CF mitigation method is demonstrated based on the commutation process. In Section III, several simulations on the CIGRE benchmark HVDC model are carried out to verify the effectiveness of the proposed method. Finally, Section IV concludes this paper.

II. PROPOSED CF MITIGATION METHOD BASED ON IMAGINARY COMMUTATION PROCESS

A. *Real Commutation Process*

According to the commutation voltage-time area [2], we have:

$$\sqrt{2}\,E\int_{\alpha}^{\alpha+\mu}\sin(\omega t)\mathrm{d}(\omega t)=X_{\mathrm{c}}\left(I_{\mathrm{d}}\left(\frac{\alpha}{\omega}\right)+I_{\mathrm{d}}\left(\frac{\alpha+\mu}{\omega}\right)\right) \tag{1}$$

where E is the root mean square (RMS) value of the commutation voltage; α is the FA; μ is the OA; X_{c} is the equivalent commutation reactance; ω is the angular frequency; $I_{\mathrm{d}}(t)$ is the DC current at time t; α/ω and $I_{\mathrm{d}}((\alpha+\mu)/\omega)$ are the beginning and ending time of commutation process, respectively.

The left side of (1) is defined as A_{su} [21], and we have:

$$A_{\mathrm{su}}=\sqrt{2}\,E\int_{\alpha}^{\alpha+\mu}\sin(\omega t)\mathrm{d}(\omega t) \tag{2}$$

where A_{su} is the supply voltage-time area, which is related to FA, OA, and E.

The right side of (1) is defined as A_{de}, and we have:

$$A_{\mathrm{de}}=X_{\mathrm{c}}\left(I_{\mathrm{d}}\left(\frac{\alpha}{\omega}\right)+I_{\mathrm{d}}\left(\frac{\alpha+\mu}{\omega}\right)\right) \tag{3}$$

where A_{de} is the demand voltage-time area of the commutation process, which is related to X_{c}, $I_{\mathrm{d}}(\alpha/\omega)$, and $I_{\mathrm{d}}((\alpha+\mu)/\omega)$.

After the fault, (2) and (3) can be rewritten as:

$$A'_{\mathrm{su}}=\sqrt{2}\,E'\int_{\alpha'}^{\alpha'+\mu'}\sin(\omega t)\mathrm{d}(\omega t) \tag{4}$$

$$A'_{\mathrm{de}}=X_{\mathrm{c}}\left(I'_{\mathrm{d}}\left(\frac{\alpha'}{\omega}\right)+I'_{\mathrm{d}}\left(\frac{\alpha'+\mu'}{\omega}\right)\right) \tag{5}$$

where $(\cdot)'$ represents the variables after the fault. The detailed analysis of commutation process is further elaborated in [21].

As for the deionization process, the EA decreases due to the increase of OA. Besides, the phase angle shift of commutation voltage $\Delta\varphi$ affects the EA. The EA γ after the fault γ' can be calculated as:

$$\gamma'=\pi-\alpha'-\mu'-\Delta\varphi \tag{6}$$

When the fault is severe or the fault is handled inappropriately, μ' would increase excessively. Thus, the EA after the fault γ' is less than the minimum EA $\gamma_{\min}$, and the CF occurs.

The real commutation process is illustrated in Fig. 1(a), where I_{dN} is the rated DC current; and $u(t)$ is the commutation voltage.

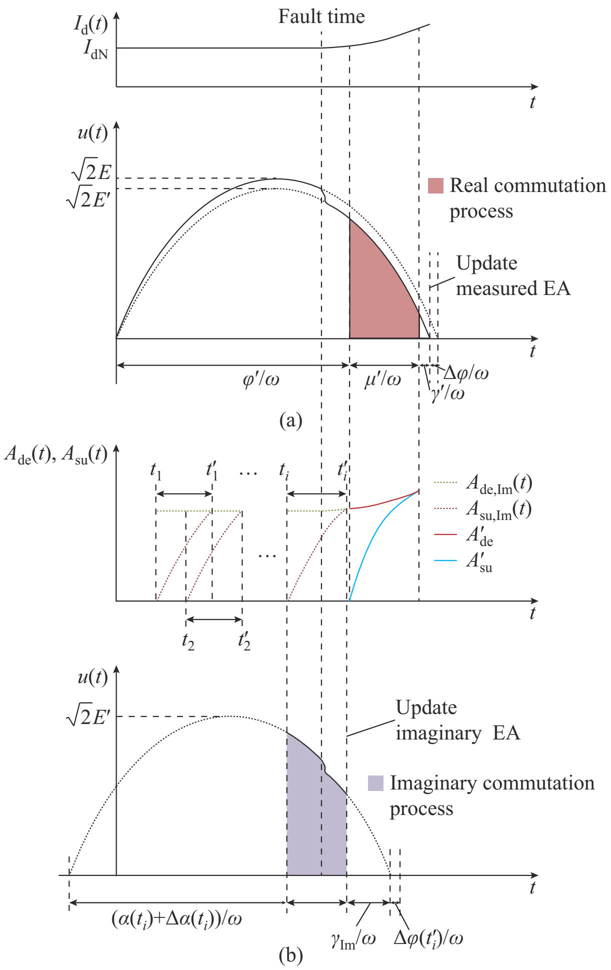

Fig. 1. Illustration of real commutation process and imaginary commutation process. (a) Waveforms corresponding to real commutation process. (b) Waveforms corresponding to imaginary commutation process considering FA shift $\Delta\alpha(t_i)$.

B. *Imaginary Commutation Process*

According to the analysis in Section II-A, the commutation process begins with the firing pulse and ends when A_{su} exceeds A_{de}. Thus, the imaginary commutation process is proposed to achieve the continuous EA calculation. The imaginary commutation process and the corresponding waveforms are shown in Fig. 1(b), where $t_i (i=1,2,\ldots)$ denotes the sampling time, which is also the beginning time of each imaginary commutation process; and $t_i' (i=1,2,\ldots)$ is the ending time of the imaginary commutation process that begins at t_i.

Before the fault occurrence, the imaginary supply voltage-time area at time t $A_{\text{su,Im}}(t)$ can be calculated as:

$$A_{\text{su,Im}}(t)=\sqrt{2}\,E\int_{\alpha(t_i)}^{\alpha(t_i)+\omega(t-t_i)}\sin(\omega t)\mathrm{d}(\omega t) \tag{7}$$

where $\alpha(t_i)$ is the FA at time t_i.

Since E may change after the fault occurrence, the real-time change of E can be considered by rewriting $A_{\text{su,Im}}(t)$ as:

$$A_{\text{su,Im}}(t)=\sqrt{2}\int_{\alpha(t_i)}^{\alpha(t_i)+\omega(t-t_i)}E(t)\sin(\omega t)\mathrm{d}(\omega t) \tag{8}$$

where $E(t)$ is the RMS value of commutation voltage at time t. In (8), the real-time change of advanced angle and $E(t)$ are considered.

Besides, the phase angle shift of commutation voltage $\Delta\varphi$ caused by the unsymmetrical faults and the active power fluctuation affects the imaginary commutation process. The impacts of phase angle shift on the commutation process can be considered from two aspects. The first impact is that the FA order is not equal to the actual FA, which results in the FA shift $\Delta\alpha$. The other impact is that the half period of commutation voltage is not equal to 10 ms, which results in the zero-crossing shift of the commutation voltage $\Delta\varphi$. Figure 2 shows the relationship between actual phase angle $\theta(t)$, system phase angle $\theta_{\text{sys}}(t)$, and normal phase angle $\theta_{\text{N}}(t)$.

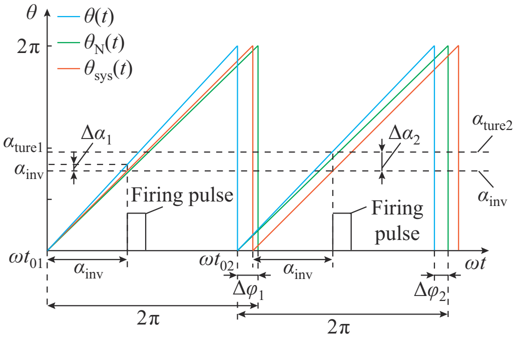

Fig. 2. Relationship between $\theta(t)$, $\theta_{\text{sys}}(t)$, and $\theta_{\text{N}}(t)$.

The actual phase angle $\theta(t)$ is the real phase angle of commutation voltage. The system phase angle $\theta_{\text{sys}}(t)$ is the output phase angle of phase-locked loop (PLL) of HVDC system. The normal phase angle $\theta_{\text{N}}(t)$ is the phase angle calculated with ωt after the commutation voltage crosses zero. Generally, the PLL of HVDC system is the synchronous reference frame phase-locked loop (SRF-PLL) [22], and the proportional and integral coefficients are too small to reduce the impact of harmonics. Thus, the dynamic response of SRF-PLL is not fast, and it takes a long time for SRF-PLL to follow the actual phase after the fault. The actual phase angle $\theta(t)$ is followed by the second order generalized integrator phase-locked loop (SOGI-PLL) [23], which has a better performance in both dynamic response and harmonic suppression.

In Fig. 2, α_{inv} is the FA order calculated by the inverter control system, and t_{01} and t_{02} are the zero-crossing time corresponding to the first and the second periods, respectively. When the system phase angle $\theta_{\text{sys}}(t)$ is equal to α_{inv}, the firing pulse is sent to the valves. Due to the phase angle shift, the system phase angle $\theta_{\text{sys}}(t)$ is not equal to the actual phase angle $\theta(t)$, leading to the FA order equaling α_{true1} and α_{true2} rather than α_{inv}. The FA shift $\Delta\alpha_1$ and $\Delta\alpha_2$ can be measured only when the firing pulse is generated. To achieve the continuous FA shift calculation, the FA shift $\Delta\alpha$ at time t can be calculated as:

$$\Delta\alpha(t)=\theta(t)-\theta_{\text{sys}}(t) \tag{9}$$

Similarly, the zero-crossing shift of the commutation voltages $\Delta\varphi_1$ and $\Delta\varphi_2$ can be measured only when the commutation voltage crosses zero. To achieve the continuous zero-crossing shift calculation caused by phase angle shift, $\Delta\varphi$ at time t can be calculated as:

$$\Delta\varphi(t)=\theta(t)-\theta_{\text{N}}(t) \tag{10}$$

$$\theta_{\text{N}}(t)=\omega(t-t_0) \tag{11}$$

where t_0 is the time when the commutation voltage crosses zero.

Considering the FA shift $\Delta\alpha(t_i)$ at the beginning time t_i of imaginary commutation process, (8) can be rewritten as:

$$A_{\text{su,Im}}(t)=\sqrt{2}\int_{\alpha(t_i)+\Delta\alpha(t_i)}^{\alpha(t_i)+\Delta\alpha(t_i)+\omega(t-t_i)}E(t)\sin(\omega t)\mathrm{d}(\omega t) \tag{12}$$

At time t, the imaginary demand voltage-time area of the commutation process $A_{\text{de,Im}}$ can be calculated as:

$$A_{\text{de,Im}}(t)=X_{\text{c}}(I_{\text{d}}(t_i)+I_{\text{d}}(t)) \tag{13}$$

The waveforms of $A_{\text{su,Im}}(t)$ and $A_{\text{de,Im}}(t)$ considering the FA shift $\Delta\alpha(t_i)$ are illustrated in Fig. 1(b). As shown in Fig. 1(b), when $A_{\text{su,Im}}(t)$ exceeds $A_{\text{de,Im}}(t)$, the imaginary commutation process that starts at t_i is completed. The ending time t_i' and the zero-crossing shift of commutation voltage $\Delta\varphi(t_i')$ are recorded. Since the deionization process is usually shorter than the commutation process, by neglecting the phase angle shift during the deionization process, the imaginary EA γ_{Im} can be calculated as:

$$\gamma_{\text{Im}}=\pi-\alpha(t_i)-\Delta\alpha(t_i)-\Delta\varphi(t_i')-\omega(t_i'-t_i) \tag{14}$$

where $\omega(t_i'-t_i)$ denotes the imaginary OA.

Equation (14) updates the imaginary EA at the end of imaginary commutation process rather than the end of deionization process, which makes it possible for the HVDC control system to act in advance.

C. Calculation of Predicted Imaginary EA with DC Current Prediction

Due to the inductances of DC transmission line and inverter-side AC transmission line, the DC current changes smoothly between the fault time and CF time. Therefore, based on the DC current and the rate of DC current variation, it is possible to predict the DC current within a short time before CF. The predicted DC current can be expressed as:

$$I_{\mathrm{d,pre}}(t_i)=I_{\mathrm{d}}(t_i)+T_{\mathrm{pre}}k_{I_{\mathrm{d}}}(t_i) \tag{15}$$

where $I_{\mathrm{d,pre}}(t_i)$, $I_{\mathrm{d}}(t_i)$, and $k_{I_{\mathrm{d}}}(t_i)$ are the predicted DC current, the DC current, and the rate of DC current variation at time t_i, respectively; and T_{pre} is the prediction time, which is adjustable.

The DC current prediction loses the accuracy after CF occurs due to the short circuit of DC terminal. However, the DC current prediction is practicable during the transient fault period before CF occurs.

Substituting (15) into (13), the predicted imaginary supply voltage-time area $A_{\mathrm{de,Im,pre}}$ can be calculated as:

$$A_{\mathrm{de,Im,pre}}(t)=X_{\mathrm{c}}\left(I_{\mathrm{d,pre}}(t_i)+I_{\mathrm{d,pre}}(t)\right) \tag{16}$$

Similarly, the ending time of predicted imaginary commutation process $t'_{i,\mathrm{pre}}$ can be acquired by comparing $A_{\mathrm{su,Im}}$ and $A_{\mathrm{de,Im,pre}}$. Based on (14), the predicted imaginary EA $\gamma_{\mathrm{Im,pre}}$ can be calculated as:

$$\gamma_{\mathrm{Im,pre}}=\pi-\alpha(t_i)-\Delta\alpha(t_i)-\Delta\varphi(t'_{i,\mathrm{pre}})-\omega(t'_{i,\mathrm{pre}}-t_i) \tag{17}$$

D. Proposed CF Mitigation Method

The two-terminal HVDC system is the most used structure consisting of a rectifier side and inverter side, each of which has its own control system. Figure 3 shows the block diagram of the HVDC control system. The rectifier-side control system includes the constant current (CC) controller and the minimum FA control, which can be realized by the PI controller. The inverter-side control system includes the CC controller, CEA, current error (CE) controller, VDCOL, and the proposed method. In Fig. 3, I_{drec}, I_{dinv}, and U_{dinv} are the rectifier-side DC current, inverter-side DC current, and inverter-side DC voltage, respectively; and u_0 is the zero-sequence voltage, and the zero-crossing time is detected by the zero-crossing detector (ZCD).

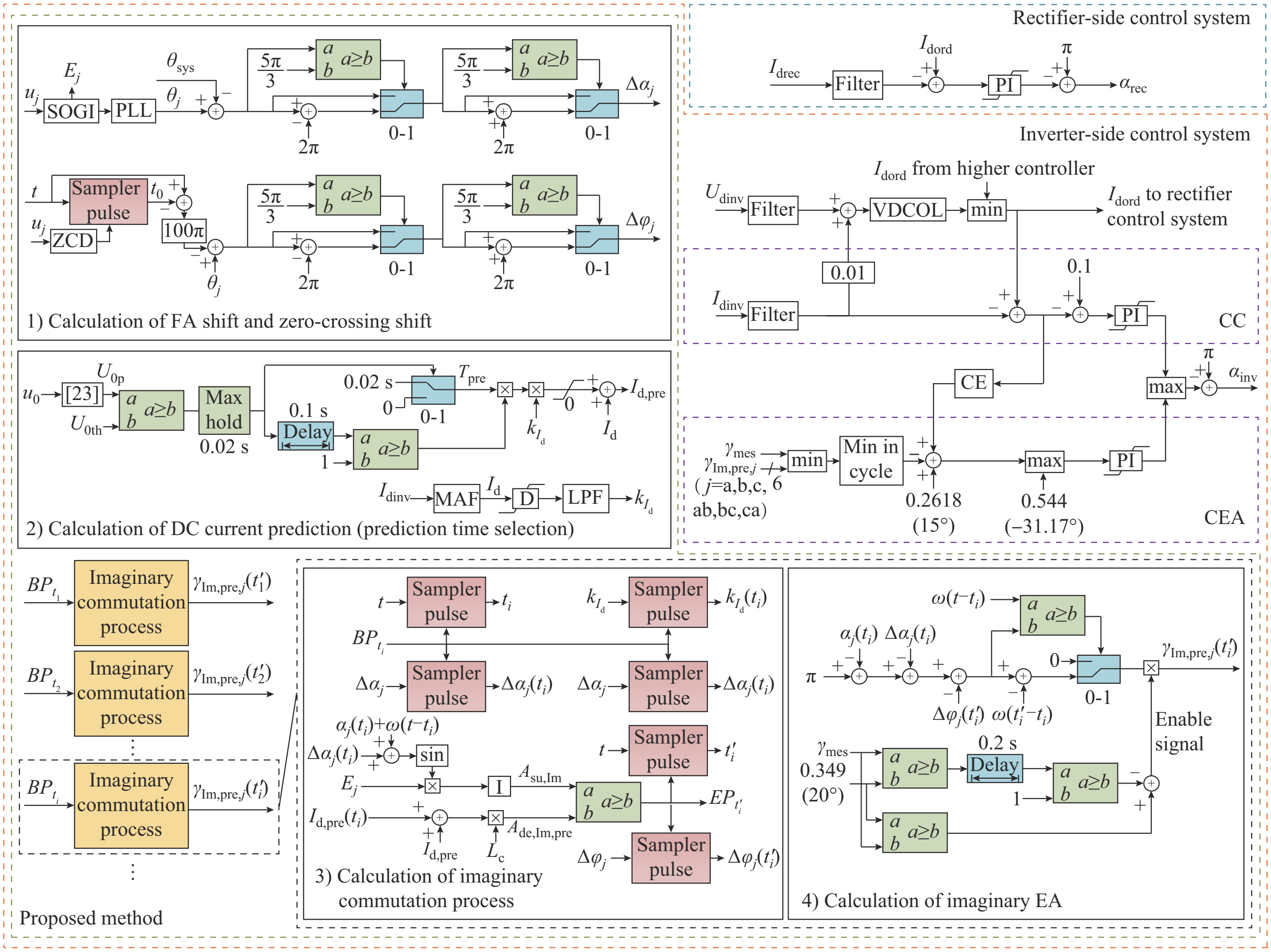

Fig. 3. Block diagram of HVDC control system with the proposed method.

To prevent the CF, the detailed procedure of the proposed method can be described as follows.

1) Calculation of FA Shift and Zero-crossing Shift

The FA shift $\Delta\alpha$ and the zero-crossing shift of the commutation voltage $\Delta\varphi$ are calculated based on (13) and (14), respectively. The comparator is used to avoid the output spike near the zero-crossing point. When $\Delta\alpha$ or $\Delta\varphi$ is larger than $5\pi/3$, the output is $\Delta\alpha-2\pi$ or $\Delta\varphi-2\pi$, respectively. When $\Delta\alpha$ or $\Delta\varphi$ is less than $-5\pi/3$, the output is $\Delta\alpha+2\pi$ or $\Delta\varphi+2\pi$, respectively.

2) Calculation of DC Current Prediction

The predicted DC current is calculated by (15). I_{d} is filtered by a moving average filtering (MAF), which has a time constant of 3.33 ms due to the specific harmonic in DC current. $k_{I_{\mathrm{d}}}$ is calculated by the derivative (D) of I_{d} and then filtered by a low-pass filter (LPF), which has a time constant of 2 ms. To better mitigate the CF, T_{pre} is selected to be 0 ms when the amplitude value of zero-sequence voltage $U_{0\mathrm{p}}$ is smaller than the threshold $U_{0\mathrm{th}}$ (0.02 p.u.), and T_{pre} is selected as 20 ms when $U_{0\mathrm{p}}$ is larger than $U_{0\mathrm{th}}$. The reason is explained in detail in Section III-C. Moreover, to avoid the DC fluctuation under the single-line-to-ground fault, T_{pre} is selected as 0 ms when $U_{0\mathrm{p}}$ is larger than $U_{0\mathrm{th}}$ for 0.1 s, which is explained in detail in Section III-D. The method proposed in [24] is used for the calculation of $U_{0\mathrm{p}}$.

3) *Calculation of Imaginary Commutation Process*

The imaginary commutation process starts with the begin pulse at t_i BP_{t_i} ($i=1, 2, \ldots$), which means there is an imaginary commutation process beginning at every sampling time of each commutation voltage u_j ($j=\mathrm{a, b, c, ab, bc, ca}$). E_j is the corresponding RMS value of u_j. The time t, the FA shift $\Delta\alpha$, the DC current I_{d}, and the rate of change of DC current $k_{I_{\mathrm{d}}}$ at time t_i are recorded. Then, the imaginary supply voltage-time area $A_{\mathrm{su,Im}}$ and the predicted imaginary demand voltage-time area $A_{\mathrm{de,Im,pre}}$ are calculated by (12) and (16), respectively. When $A_{\mathrm{su,Im}}$ is larger than $A_{\mathrm{de,Im,pre}}$, the imaginary commutation process beginning at time t_i is completed. Meanwhile, the end pulse at t_i' $EP_{t_i'}$ is generated to record the time t and the zero-crossing shift $\Delta\varphi$ at time t_i'.

4) *Calculation of Imaginary EA*

The predicted imaginary EA $\gamma_{\mathrm{Im,pre}}$ is calculated by (17). Since there is a predicted imaginary EA corresponding to every imaginary commutation process, the predicted imaginary EA can be continuous.

Both the predicted imaginary EA and the measured EA are set as the input of the CEA controller. Besides, to reduce the side effect of the predicted imaginary EA on the recovery process, the proposed method is blocked when the measured EA is larger than 20° for 20 ms and is enabled when the imaginary EA is less than 20°, as shown in Fig. 4. The detailed reason is explained in Section III-B.

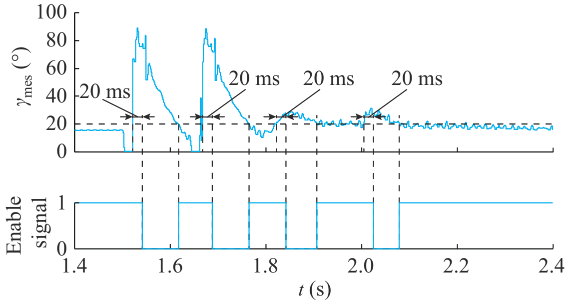

Fig. 4. Generation of enable signal of proposed method.

III. Simulation and Results

A. *Test Model*

To validate the effectiveness of the proposed method, several simulations have been performed in the CIGRE benchmark HVDC model based on the PSCAD/EMTDC [13]. The parameters of the test network are listed in Table I. The simulation step is 10 μs, and the sampling step and control step are both 100 μs.

TABLE I
Parameters of Test Network

Test network	Item	Value	
		Rectifier side	Inverter side
AC system	AC voltage (kV)	382.87	215.05
	SCR	2.5	2.5
	Reactive compensation (Mvar)	626	626
	Transformer ratio	345 kV/213.5 kV	230 kV/209.2 kV
	Transformer leakage inductance (p.u.)	0.18	0.18
DC system	DC resistance (Ω)	5	
	DC inductance (H)	1.2	
	Rated DC voltage (kV)	500	
	Rated DC current (kA)	2	

B. *Calculation Accuracy of Imaginary EA*

Figure 5 shows the results of the proposed calculation method of imaginary EA under single-phase line-to-ground (A-G) and three-phase line-to-ground (ABC-G) faults with different fault inductances L_{f}. In all cases, the fault is applied at $t=1.500$ swith a duration of 0.05 s. Only the proposed calculation method of imaginary EA is applied to evaluate the accuracy, and the imaginary EA is not added into the CEA controller.

Referring to Fig. 5, different from the step change of the measured EA, the imaginary EA changes gradually with DC current, commutation voltage, FA shift, and zero-crossing shift of the commutation voltage.

Due to the measurement delay and phase-locked error, the calculation error of imaginary EA is inevitable. However, the variation tendency of the imaginary EA coincides with that of the measured EA after the fault. Because the rate of DC current variation is not zero after the fault, the imaginary EA when $T_{\mathrm{pre}}=5$ ms changes earlier than that when $T_{\mathrm{pre}}=0$ ms. Since the imaginary EA changes earlier than the measured EA, it is possible for CEA controller to reduce the FA earlier to prevent CF. The spike of the imaginary EA in Fig. 5 is caused by the sudden change of the FA along with the update of the measured EA.

It should be noted that the imaginary EA is updated earlier than the measured EA all the time. So, with the proposed method, the FA decreases at the beginning of the fault to improve the CF mitigation performance. However, it would slow down the recovery process since the FA increases later. Thus, to reduce the side effect of the proposed method during the recovery process, the proposed method is blocked when the measured EA is larger than 20° for a duration of 20 ms, which makes sure that the HVDC system is under recovery process and at a low risk of CF. Moreover, the proposed method is enabled immediately after the imaginary EA is less than 20°. This is because the measured EA is usually larger than 20° immediately after the fault and tends to be smaller than 20° when the HVDC system is recovering to equilibrium operation point.

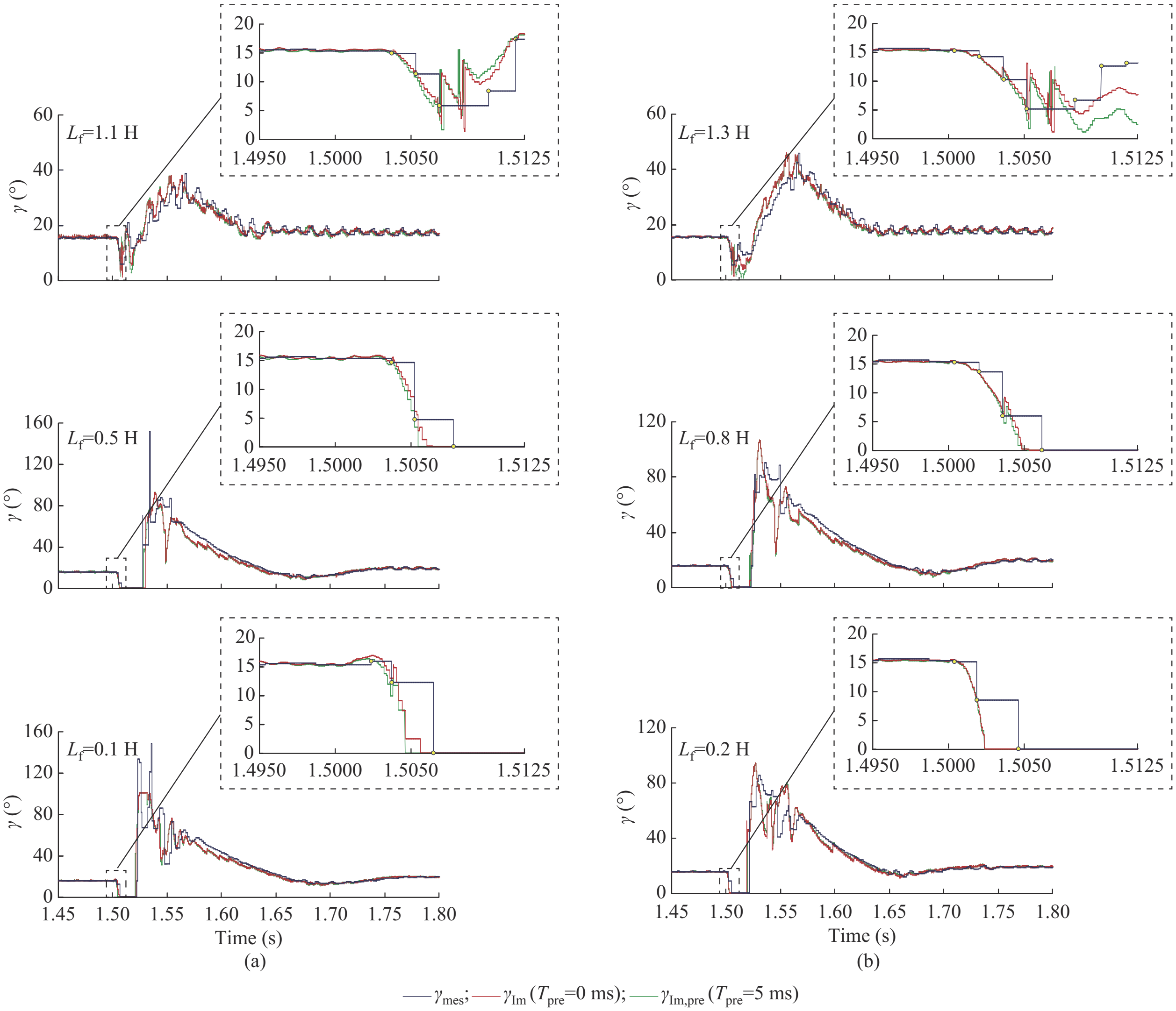

(a)

(b)

Fig. 5. Waveforms of imaginary EA (γ_{Im} ($T_{\mathrm{pre}}=0$ ms) and $\gamma_{\mathrm{Im,pre}}$ ($T_{\mathrm{pre}}=5$ ms)) and measured EA γ_{mes} under different faults. (a) A-G faults with different Lf. (b) ABC-G faults with different L_f.

C. CF Mitigation Performance of Proposed Method

Figure 6 shows the system response under the A-G and ABC-G faults with CIGRE control and the proposed method. In both cases, the fault is applied at $t=1.500$ s with a duration of 0.1 s. The L_f is 0.7 H and $T_{\mathrm{pre}}=20$ ms under the A-G fault. The L_f is 1.1 H and $T_{\mathrm{pre}}=0$ ms under the ABC-G fault. Moreover, the commutation processes CP1-CP12 of different commutation voltages are defined in Appendix A.

When an A-G fault occurs, the risk of CF increases under the joint action of voltage drop, DC current rise, and phase angle shift of the commutation voltage. With the CIGRE control, the measured EA updates when the commutation voltage crosses zero, resulting in a distinct delay. Referring to the blue lines in Fig. 6(a), when the CF occurs, the DC voltage drops massively, and the DC current increases to 2.4 p. u.. As can be observed, the measured EA updates to 14.79° and 8.65° at 1.5037 s and 1.5053 s, respectively, which makes FA update to 141.38° and 136.76°. However, the FA order 141.37° sent to the system at 1.5049 s, which is the firing time of CP4, as shown in Appendix A Fig. A2, is not small enough to supply a sufficient voltage-time area to avoid the upcoming CF. Thus, the delay of the EA measurement restricts the ability to mitigate CF.

Referring to the red lines in Fig. 6(a), with the DC current prediction, the imaginary EA changes much earlier than the measured EA, resulting in the fast reaction of CEA control. The imaginary EA updates to 13.29° and 5.08° at 1.5037 s and 1.5053 s, which makes FA update to 140.26° and 133.84°, respectively. And the FA order 135.66° sent to the system at 1.5049 s, which is the firing time for CP4, is 5.71° less than that of CIGRE control, makes it possible for the completion of commutation process. As the FA is reduced quickly after the fault, the CF is mitigated. The same analysis can be extended to ABC-G fault, as shown in Fig. 6(b).

To investigate the impact of fault time on the CF mitigation performance of the proposed method, several simulations are conducted. The AC faults are applied at different time, which varies from 1.500 s to 1.509 s with the time step of 0.001 s.

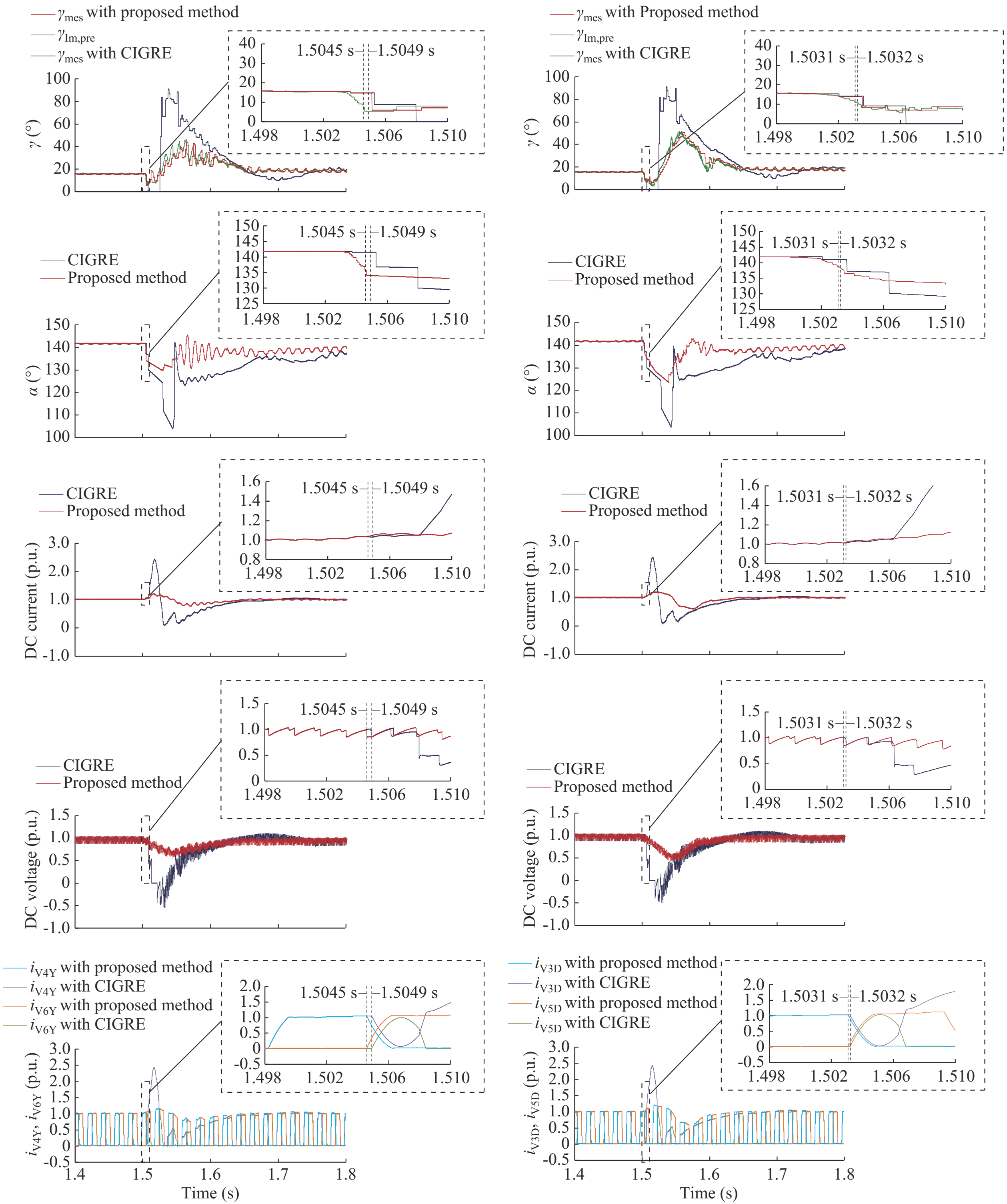

(a) (b)

Fig. 6. System response under different faults with different control methods. (a) A-G fault. (b) ABC-G fault.

The simulation results under A-G and ABC-G faults with different control methods are shown in Fig. 7(a) and (b), respectively, where L_{fmin} denotes the minimum value of fault inductance, corresponding to the most severe fault when the CF does not occur. It can be observed from Fig. 7 that the proposed method has a better performance in mitigating CF than CIGRE control regardless of T_{pre}, and the proposed method has a better performance in mitigating CF than the method in [19] when T_{pre} is selected properly.

Under the A-G faults, the CF mitigation of CIGRE control or the proposed method with different T_{pre} acts differently at different fault time.

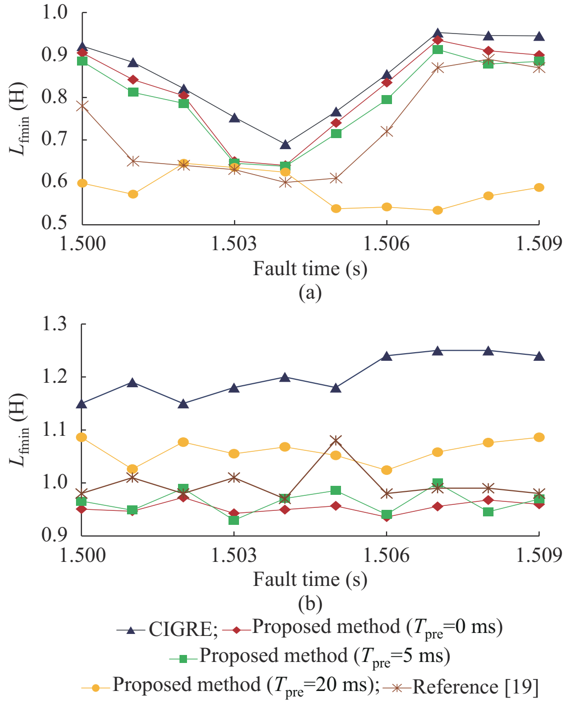

Fig. 7. Performance of CF mitigation under different faults with different control methods. (a) A-G faults. (b) ABC-G faults.

As can be observed from Fig. 7(a) and Appendix A Fig. A2, with the CIGRE control, the CF mitigation ability firstly increases with the increment of the time interval from the fault time to CP4. This is because it takes a quite short time (about several milliseconds, depends on the fault severity) for the voltage to drop after the fault. When the fault time are far from CP4, the commutation processes before CP4 are less affected, which means the corresponding EA are deduced a little. Therefore, the FA order will not be deduced properly to enlarge the supply voltage-time area of CP4. Thus, CF occurs at CP4. Therefore, the CF mitigation ability depends on CP4 and CP5 when fault time is during 1.500-1.503 s. However, if the fault time is around 1.504 s or after 1.504 s, the supply voltage-time area of CP4, CP5, and CP6 will not be affected as much as that when voltage drops for a while. Therefore, the CF mitigation ability depends on CP10 and CP11 when fault time is from 1.504 s to 1.509 s. During 1.504-1.509 s, when the fault time is closer to 1.504 s, CP4, CP5, and CP6 are more affected, which means the corresponding EA is deduced more. Therefore, the FA order will be smaller and the supply voltage-time area of CP10 and CP11 will be larger. Thus, the CF mitigation ability decreases with the increment of the time interval from the fault time to CP4, and the CF mitigation ability is the highest when the fault time is just before CP4, i.e., 1.504 s. Therefore, even with the proposed method, the improvement of CF mitigation performance is not obvious at 1.504 s.

Moreover, the DC current prediction time T_{pre} is selected as 20 ms considering the DC current measurement delay caused by MAF, the variation rate of DC calculation delay caused by LPF, and the fact that CF mitigation ability depends on CP10 and CP11 when the fault time is around CP4 and CP5, which has a time interval of about 10 ms.

Under the A-G faults, the proposed method with $T_{\mathrm{pre}}=20$ ms can update EA earlier and quicklier than that with $T_{\mathrm{pre}}=5$ ms or 0 ms. Thus, even if the fault initial time is far from CP4 such as 1.500 s, the FA with $T_{\mathrm{pre}}=20$ ms will be decreased to mitigate the upcoming CF of CP4. With the proposed method with $T_{\mathrm{pre}}=20$ ms, the CF mitigation ability is largely increased when the fault initial time ranged during 1.500-1.502 s and 1.506-1.509 s. However, if T_{pre} is selected larger than 25 ms, the CF mitigation performance of the proposed method would be worse. It is because the excessively reduced FA decreases the AC voltage and then increases the DC current, and the FA control does more harm than good in this situation. Still, the CF mitigation can be improved with DC current control or reactive power compensation equipment since the CF time is largely postponed.

Under the ABC-G faults, the commutation process of every valve is equally affected by the fault time. The voltage drop and the phase angle shift of every commutation voltage are equally changed as well. In this situation, the EA corresponding to every commutation process tends to decrease. If $T_{\mathrm{pre}}=0$ ms or 5 ms, the predicted imaginary EA updates a little earlier than the measured EA. Thus, the FA generated by CEA controller is appropriate to mitigate CF. When $T_{\mathrm{pre}}=20$ ms, the predicted imaginary EA updates earlier and decreases more than that when $T_{\mathrm{pre}}=0$ ms or 5 ms. Thus, the FA is reduced more and earlier, which tends to increase the DC current and decrease the AC voltage. Moreover, both the voltage sag and the DC current increment are severer than that of A-G faults. The FA is reduced more when $T_{\mathrm{pre}}=0$ ms or 5 ms than $T_{\mathrm{pre}}=20$ ms.

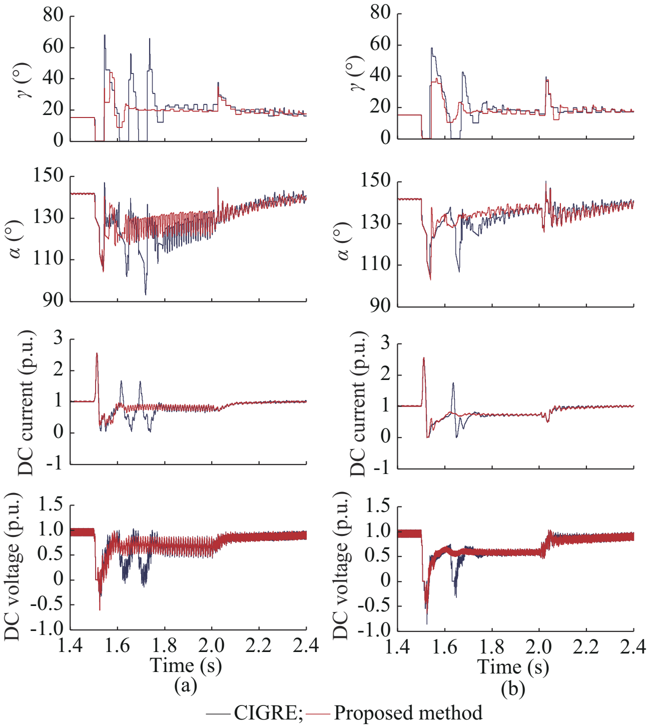

Fig. 8. System response under different faults with different control methods. (a) A-G fault. (b) ABC-G fault.

D. Subsequent CF Mitigation Performance of Proposed Method

Figure 8 shows the system response under the A-G and ABC-G faults with CIGRE control and the proposed method. In both cases, the fault is applied at $t=1.500$ s with a duration of 0.5 s. The L_{f} are 0.2 H and 0.15 H under the A-G and ABC-G faults, respectively.

It can be observed from Fig. 8 that the proposed method can mitigate subsequent CF effectively. It should be noted that, due to the second harmonic value of DC current under the unsymmetrical fault [8], T_{pre} is selected as 0 ms when the zero-sequence voltage is larger than the threshold with a duration of 0.1 s. Otherwise, the second harmonic value of DC current would cause an oscillation in predicted EA and then make FA oscillate as well.

IV. Conclusion

In this paper, the imaginary commutation process is analyzed by commutation voltage-time area, and a CF mitigation method based on the imaginary commutation process is proposed. In the proposed method, the variation of AC voltage, DC current, FA shift, and the zero-crossing shift are considered. By analyzing the simulation results of the CIGRE benchmark model built in PSCAD/EMTDC, it can be concluded that:

1) The proposed calculation method of imaginary EA can calculate the EA quickly and accurately during the transient fault process.

2) The proposed method can improve the system CF mitigation capability under AC faults, especially under A-G faults. Under the A-G faults, the system has better CF mitigation performance when $T_{\mathrm{pre}}=20$ ms than 0 ms. Under the ABC-G faults, the system has better CF mitigation performance when $T_{\mathrm{pre}}=0$ ms than 20 ms.

3) The proposed method can also mitigate subsequent CF.

Appendix A

In Table AI, $k_{\mathrm{Y/D}}$ and $k_{\mathrm{Y/Y}}$ are the transformer ratios of Y/D transformer and Y/Y transformer, respectively; $i_{\mathrm{V}n}$ is the currents flowing through valve VT_n ($n=1, 2, ..., 6$); and the subscripts D and Y represent the variables of Y/D and Y/Y transformers, respectively.

TABLE AI
Commutation Voltage of Different Commutation Processes

Transformer	Commutation process	Commutation voltage
Y/D	$\mathrm{V_{1D}}$ - $\mathrm{V_{3D}}$ (CP11)	$k_{\mathrm{Y/D}}U_{\mathrm{a}}$
	$\mathrm{V_{3D}}$ - $\mathrm{V_{5D}}$ (CP3)	$-k_{\mathrm{Y/D}}U_{\mathrm{b}}$
	$\mathrm{V_{5D}}$ - $\mathrm{V_{1D}}$ (CP7)	$-k_{\mathrm{Y/D}}U_{\mathrm{c}}$
	$\mathrm{V_{2D}}$ - $\mathrm{V_{4D}}$ (CP1)	$k_{\mathrm{Y/D}}U_{\mathrm{c}}$
	$\mathrm{V_{4D}}$ - $\mathrm{V_{6D}}$ (CP5)	$k_{\mathrm{Y/D}}U_{\mathrm{a}}$
	$\mathrm{V_{6D}}$ - $\mathrm{V_{2D}}$ (CP9)	$k_{\mathrm{Y/D}}U_{\mathrm{b}}$
Y/Y	$\mathrm{V_{1Y}}$ - $\mathrm{V_{3Y}}$ (CP10)	$k_{\mathrm{Y/Y}}(U_{\mathrm{b}}-U_{\mathrm{a}})$
	$\mathrm{V_{3Y}}$ - $\mathrm{V_{5Y}}$ (CP2)	$k_{\mathrm{Y/Y}}(U_{\mathrm{c}}-U_{\mathrm{b}})$
	$\mathrm{V_{5Y}}$ - $\mathrm{V_{1Y}}$ (CP6)	$k_{\mathrm{Y/Y}}(U_{\mathrm{a}}-U_{\mathrm{c}})$
	$\mathrm{V_{2Y}}$ - $\mathrm{V_{4Y}}$ (CP12)	$k_{\mathrm{Y/Y}}(U_{\mathrm{c}}-U_{\mathrm{a}})$
	$\mathrm{V_{4Y}}$ - $\mathrm{V_{6Y}}$ (CP4)	$k_{\mathrm{Y/Y}}(U_{\mathrm{a}}-U_{\mathrm{b}})$
	$\mathrm{V_{6Y}}$ - $\mathrm{V_{2Y}}$ (CP8)	$k_{\mathrm{Y/Y}}(U_{\mathrm{b}}-U_{\mathrm{c}})$

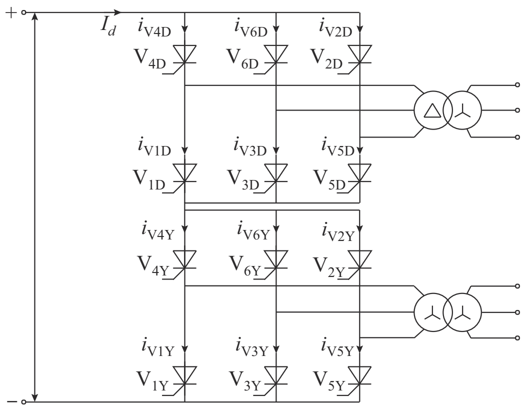

Fig. A1. Twelve-pulse converter at inverter side.

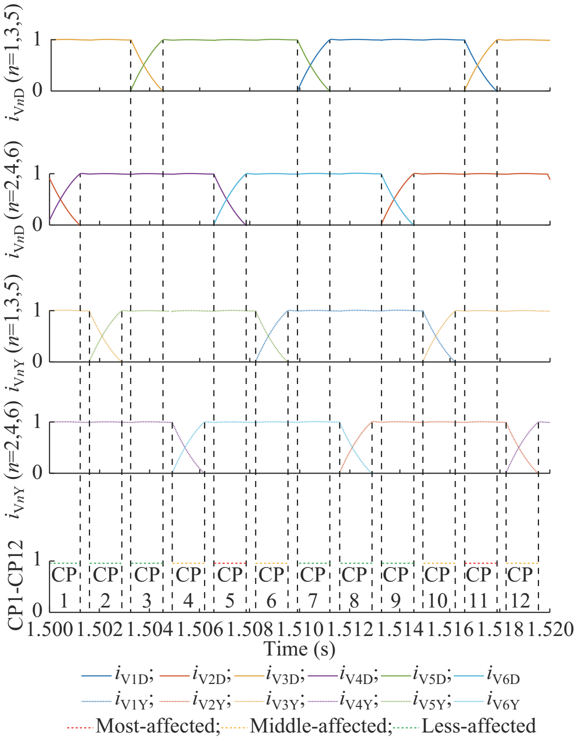

Fig. A2. Commutation process.

References

[1] T. Wu, Y. Zheng, Q. Liu *et al.*, “Continuous commutation failure suppression method based on self-adaptive auto-disturbance rejection proportional-integral controller for HVDC transmission system,” *Journal of Modern Power Systems and Clean Energy*, vol. 8, no. 6, pp. 1178-1187, Nov. 2020.

[2] L. Jing, Bin Wang, X. Dong *et al.*, “An overview of continuous commutation failure in HVDC transmission system,” *Electric Power Automation Equipment*, vol. 39, no. 9, pp. 116-122, Jan. 2019.

[3] C. Guo, B. Liu, and C. Zhao, “Improved coordinated control approach for evolved CCC-HVDC system to enhance mitigation effect of commutation failure,” *Journal of Modern Power Systems and Clean Energy*, vol. 9, no. 2, pp. 338-346, Mar. 2021.

[4] S. Ruan, K. Xu, D. Liu *et al.*, “Statistical analysis and suggestions on resistance measures for commutation failures of HVDC transmission system,” *Automation of Electric Power Systems*, vol. 43, no. 18, pp. 13-17, Sept. 2019.

[5] B. Rehman, C. Liu, H. Li *et al.*, “Analysis on local and concurrent commutation failure of multi-infeed HVDC considering inter-converter interaction,” *Journal of Modern Power Systems and Clean Energy*, vol. 10, no. 4, pp. 1050-1059, Jul. 2022.

[6] Q. Tao and Y. Xue, "Quantitative assessment for commutation security based on extinction angle trajectory," *Journal of Modern Power Systems and Clean Energy*, vol. 9, no. 2, pp. 328-337, Mar. 2021.

[7] H. Xiao, Y. Li, J. Zhu *et al*., "Efficient approach to quantify commutation failure immunity levels in multi-infeed HVDC systems," *IET Generation, Transmission & Distribution*, vol. 10, no. 4, pp. 1032-1038, Mar. 2016.

[8] L. Zeng, Y. Li, Y. Zhang *et al*., "Research on mechanism and control strategy of continuous commutation failures in HVDC system caused by asymmetrical fault in inverter-side AC system," *Proceedings of the CSEE*, vol. 39, no. 11. pp. 3159-3168, Jun. 2019.

[9] Y. Xue and X. Zhang, "Reactive power and AC voltage control of LCC HVDC system with controllable capacitors," *IEEE Transactions on Power Systems*, vol. 32, no.1, pp. 753-764, Jan. 2017.

[10] Q. Meng, Z. Liu, L. Hong *et al*., "A suppression method based on nonlinear VDCOL to mitigate the continuous commutation failure," *Power System Protection and Control*, vol. 47, no. 7, pp. 119-127, Apr. 2019.

[11] H. Zhou, W. Yao, C. Li *et al*., "A predictive voltage dependent current order limiter with the ability to reduce the risk of first commutation failure of HVDC," *High Voltage Engineering*, doi: 10.13336/j.1003-6520.hve.20210532.

[12] Z. Wei, W. Fang, and J. Liu, "Variable extinction angle control strategy based on virtual resistance to mitigate commutation failures in HVDC system," *IEEE Access*, vol. 8, pp. 93692-93704, May 2020.

[13] M. O. Faruque, Y. Zhang, and V. Dinavahi, "Detailed modeling of CIGRE HVDC benchmark system using PSCAD/EMTDC and PSB/SIMULINK," *IEEE Transactions on Power Delivery*, vol. 21, no. 1, pp. 378-387, Jan. 2006.

[14] S. Wang, S. Lu, Y. Hou *et al*., "Improvement of HVDC commutation failure response based on compound phase-shifting control," *Journal of Engineering*, vol. 2017, pp. 1473-1477, Dec. 2017.

[15] S. Mirsaeidi and X. Dong, "An enhanced strategy to inhibit commutation failure in line-commutated converters," *IEEE Transactions on Industrial Electronics*, vol. 67, no. 1, pp. 340-349, Jan. 2020.

[16] H. Wang, Y. Huang, and Q. Zhou, "Analysis of commutation failure response strategies and prediction control technology in HVDC," *Power System Protection and Control*, vol. 42, no. 21, pp. 125-131, Nov. 2014.

[17] L. Zhang and L. Dofnas, "A novel method to mitigate commutation failures in HVDC systems," in *Proceedings of International Conference on Power System Technology*, Kunming, China, Oct. 2002, pp. 51-56.

[18] J. Wang, Zi. Wang, X. Xuan *et al*., "Extinction angle control based on predictive calculation and its improvement," *Power System Technology*, vol. 42, no. 12, pp. 3985-3991, Dec. 2018.

[19] L. Liu, S. Lin, P. Sun *et al*., "A calculation method of Pseudo extinction angle for commutation failure mitigation in HVDC," *IEEE Transactions on Power Delivery*, vol. 34, no. 2, pp. 777-779, Apr. 2019.

[20] R. Zhu, X. Zhou, H. Xia *et al*., "A commutation failure prediction and mitigation method," *Journal of Modern Power Systems and Clean Energy*, vol. 10, no. 3, pp. 779-787, May 2022.

[21] R. Zhu, X. Zhou, H. Yin *et al*., "Commutation failure analysis considering the frequency response of transmission line," in *Proceedings of 2021 IEEE 2nd China International Youth Conference on Electrical Engineering (CIYCEE)*, Chengdu, China, Dec. 2021, pp. 1-6.

[22] Q. Wu, C. Fu, Y. Gong *et al*., "Comparative analysis of three kinds of HVDC synchronous firing control systems," *Power System Technology*, vol. 44, no. 12, pp. 4744-4754, Dec. 2020.

[23] M. Ciobotaru, R. Teodorescu, and F. Blaabjerg, "A new single-phase PLL structure based on second order generalized integrator," in *Proceedings of IEEE Power Electronics Specialists Conference (PESC' 06)*, Jeju, South Korea, Jun. 2006, pp. 1-6,

[24] L. Xiong, F. Zhuo, M. Zhu *et al*., "Research on fast phase synchronization in single-phase power systems," *Proceedings of the CSEE*, vol. 35, no. 9, pp. 2209-2216, May 2015.

Renlong Zhu received the B.S. degree from the College of Electrical and Information Engineering, Hunan University, Changsha, China, in 2018. He has been working towards the Ph.D. degree in electrical engineering in the College of Electrical and Information Engineering, Hunan University, since 2020. His research interests include modeling and control of line commutated converter based high-voltage direct current (LCC-HVDC) and voltage source converter based high-voltage direct current (VSC-HVDC).

Xiaoping Zhou received the B.S., M.S., and Ph.D. degrees from the College of Electrical and Information Engineering, Hunan University, Changsha, China, in 2009, 2013, and 2018, respectively. Currently, he is a full-time Associate Professor in electrical engineering from Hunan University. His research interests include high-voltage direct current (HVDC), power electronics, distributed generation, and microgrid.

Haitao Xia received the B.Eng. degree from the College of Electrical and Information Engineering, Hunan University, Changsha, China, in 2017. He has been working towards the Ph.D. degree in electrical engineering in the College of Electrical and Information Engineering, Hunan University, since 2019. His research interests include high-voltage direct current (HVDC) and dynamic analysis of power electronics converters.

Lerong Hong received the B.Eng. and Ph.D. degrees from the College of Electrical and Information Engineering, Hunan University, Changsha, China, in 2016 and 2021, respectively. He has been working as Post Doctor in electrical engineering in the College of Electrical and Information Engineering, Hunan University. His research interests include high-voltage direct current (HVDC) and power electronic converters.

Hanhang Yin received the B.Eng. degree from the College of Electrical and Information Engineering, Hunan University, Changsha, China, in 2018. She has been working toward the Ph.D. degree in electrical engineering in the College of Electrical and Information Engineering, Hunan University, since 2020. Her research interests include power electronic converter modeling, stability analysis, and modular multilevel converter (MMC).

Lingfeng Deng received the B.S. degree from the College of Electrical and Power Engineering, China University of Mining and Technology, Xuzhou, China, in 2018 and the M.S. degree from the College of Electrical and Information Engineering, Hunan University, Changsha, China, in 2021. He has been working towards the Ph.D. degree in electrical engineering in the College of Electrical and Information Engineering, Hunan University, since 2021. His research interests include high-voltage direct current (HVDC) and dynamic analysis of power electronics converters.

Yifeng Liu received the B.S. degree in electrical engineering from the Hunan Institute of Engineering, Xiangtan, China, in 2016. He has been working towards the Ph.D. degree in electrical engineering in the College of Electrical and Information Engineering, Hunan University, Changsha, China, since 2019. His research interests include modeling and control of power electronic converters, distributed generation, and high-voltage direct current (HVDC).